Published in final edited form as:
Magn Reson Med. 2003 September ; 50(3): 638–642.

Assessment of Regional Systolic and Diastolic Dysfunction in Familial Hypertrophic Cardiomyopathy Using MR Tagging

Daniel B. Ennis[1,2,*], **Frederick H. Epstein**[2,3], **Peter Kellman**[2], **Lameh Fananapazir**[2], **Elliot R. McVeigh**[1,2], and **Andrew E. Arai**[2]

[1]*Department of Biomedical Engineering, Johns Hopkins University School of Medicine, Baltimore, Maryland.* [2]*National Heart, Lung, and Blood Institute, National Institutes of Health, Bethesda, Maryland.* [3]*Department of Radiology, University of Virginia, Charlottesville, Virginia.*

Abstract

Diastolic and systolic left ventricular (LV) dysfunction often significantly contribute to disabling symptoms in familial hypertrophic cardiomyopathy (FHC). This study compares regional LV function (midwall circumferential strain) during systole and diastole in eight FHC patients and six normal volunteers (NVs) using MR tagging. A prospectively-gated fast gradient-echo sequence with an echo-train readout was modified to support complementary spatial modulation of magnetization (CSPAMM) tagging and full cardiac cycle data acquisition using the cardiac phase to order reconstruction (CAPTOR), thus providing tag persistence and data acquisition during the entire cardiac cycle. Total systolic strains in FHC patients were significantly reduced in septal and inferior regions (both $P < 0.01$). Early-diastolic strain rates were reduced in all regions of the FHC group (all $P < 0.03$). The combination of CSPAMM and CAPTOR allows regional indices of myocardial function to be quantified throughout the cardiac cycle. This technique reveals regional differences in systolic and diastolic impairment in FHC patients.

Keywords

hypertrophy; cardiomyopathy; diastole; tagging; regional

Familial hypertrophic cardiomyopathy (FHC) is a genetic disease characterized by left ventricular (LV) hypertrophy and myofiber disarray. LV diastolic dysfunction is common and contributes importantly to congestive heart failure. To accurately assess regional function, it is necessary to obtain local measures of myocardial shortening and relaxation. Magnetic resonance (MR) tissue tagging is a proven method for imaging myocardial systolic function (1,2). Tagging has been used to assess systolic function in NVs (3,4) and patients with diseases such as hypertrophic cardiomyopathy (5-7), aortic stenosis (8), and coronary artery disease (9).

Most tagging techniques are limited by two factors: tag fading and trigger windowing. T_1 relaxation causes the tags to fade to undetectable levels by early diastole (~500 ms). This typically limits both qualitative and quantitative assessment of myocardial tag motion to systole. In order to characterize indices of regional LV function in FHC, the CSPAMM (10) tagging technique, which provides tag persistence during systole and diastole, was combined with CAPTOR (11), which provides acquisition and reconstruction of cine tagged images

*Correspondence to: Daniel Ennis, Laboratory of Cardiac Energetics, National Heart, Lung, and Blood Institute, National Institutes of Health, 10 Center Drive, Bldg. 10, Rm. B1D-416, Bethesda, MD 20892. E-mail: dennis@bme.jhu.edu

across the entire cardiac cycle. The combination of these two techniques may prove valuable in assessing regional cardiac function for other diseases in which both systolic and diastolic dysfunction occur.

METHODS

All procedures were conducted in accordance with institutional guidelines that required signed, informed consent.

Study Population

Study populations were matched for both age and sex. In patients with FHC, CAPTOR/CSPAMM images were obtained as additional acquisitions to a standard protocol aimed at assessing global and regional function and measuring myocardial mass. FHC was defined as regional LV hypertrophy with a maximal end-diastolic wall thickness ≥ 15 mm in the absence of secondary causes, or > 20 mm for patients with one secondary cause of hypertrophy. Normal volunteers (NVs) were recruited to match the range of patient ages encountered. The volunteers had a normal cine MRI and no history of heart disease.

The patient group consisted of six men and two women (mean age = 39.0 ± 16.0 years; range = 20–64 years). The NV group consisted of four men and two women (mean age = 33.0 ± 10.3 years; range = 25–53 years, P = NS). Heart rates were 67 ± 10 beats per minute in patients with FHC, and 63 ± 7 beats per minute in NVs (P = NS).

All but one patient had symptomatic FHC, and the average New York Heart Association (NYHA) class was 2.5 ± 1.1. The average LV outflow tract gradient was 47 ± 48 mmHg at rest and 89 ± 53 mmHg with provocation. One patient had an abnormal pulmonary capillary wedge pressure (>12 mmHg) and a pseudonormalized transmitral E/A velocity ratio, indicating that from a heart failure perspective this group of patients was reasonably well compensated. Four other patients had abnormal transmitral E/A velocity ratios. A summary of the patients' anatomical measures obtained from cine MRI is provided in Table 1.

MRI

Scans were performed on a GE 1.5T cardiac MRI scanner (General Electric Medical Systems, Milwaukee, WI) using a four-element cardiac phased array coil. All subjects were monitored with a three-lead electrocardiogram. The CSPAMM tagging pulses were implemented in a cardiac-gated, fast gradient-recalled echo sequence using an echo-train readout (FGRE-ET) (12,13). The sequence also supported full cardiac phase to order reconstruction (CAPTOR). The scan parameters used were as follows: field of view (FOV) = 32–36 cm; slice thickness = 8 mm; phase FOV factor = 0.75; acquisition matrix = 160 × 128 (frequency × phase); repetition time (TR) = 30 ms; views per segment = 8; echo train length = 8; asymmetric partial k-space coverage (NEX = 0.75); and receiver bandwidth = ± 62.5 kHz. Data from the first two heartbeats were discarded. The imaging flip angle was ramped as specified by Fischer et al. (10). The total tagging flip angle was 135° with tag spacing of 7 pixels. The acquisition of a single slice required 20 heartbeats. Thirty cardiac phases were reconstructed across the cardiac cycle. Four to six mid-ventricular short-axis slices were acquired in <30 min. In NVs, eight to 10 short-axis slices and six to eight radially prescribed long-axis slices were acquired. Each direction of stripe tags was acquired in a separate breath-hold in all subjects. Conventional cine MRI was obtained in the long and short axis using both fast gradient-echo and steady-state free-precession (SSFP) methods. LV mass and wall thickness were measured by computer-assisted planimetry. Transmitral E/A velocity was measured by MR phase-contrast methods.

Image Reconstruction, Processing, and Analysis

CAPTOR sorting of the raw data was implemented on-line, and CAPTOR/CSPAMM image reconstruction was performed off-line using MATLAB (Mathworks, Natick, MA). Individual SPAMM images were reconstructed using homodyne demodulation (14), and the resultant real images were subtracted to produce the final CSPAMM image at each cardiac phase.

For the subsequent analysis, through-plane motion was neglected in the patients with FHC, with the exception of two cases in which time permitted the acquisition of long-axis tagged images. Long-axis anatomical images were used to quantify the extent of through-plane motion in all FHC patients for whom long-axis tagged images were not available. The analysis incorporated longitudinal averaging of results across mid-ventricular short-axis slices, further reducing the impacts of through-plane motion and also decreasing the noise of the quantified metrics.

The tagged CSPAMM images were processed to produce quantitative strain measures in a three-step process. First, the images were segmented using custom three-dimensional (3D) spatial and temporal template interpolation software (15). The segmentation process simplified the tag detection process by isolating the myocardium. Next, the tags were tracked nearly automatically, due to the high contrast, using the FindTags program (16). Finally, the tag displacements were fitted using a multidimensional B-spline tensor product, resulting in a material coordinate displacement field from which material (Lagrangian) strains were calculated for a sequence of time points throughout the cardiac cycle (17). Circumferential strains from the midwall of the LV were analyzed. This strain component is physiologically meaningful, as it aligns well with the local myofiber direction and is well characterized by short-axis tagged images. Regional analysis of function was performed by averaging strain results within four ventricular segments, defined as follows. The septal segment was defined as any septal myocardium lying between the anterior and inferior insertions of the right ventricle onto the LV. The anterior, lateral, and inferior segments were defined clockwise as the first one-third, second one-third, and last one-third of the remaining myocardial wall.

Evaluation of Regional LV Function

LV regional midwall circumferential strain (E_{CC}) curves from each subject were used to characterize two indices of systolic function and five indices of diastolic function. All indices are described in Fig. 1 for a myocardial segment from a NV and a patient with FHC. The systolic strain rate was defined as the slope of the E_{CC} curve from end-diastole to 90% of the peak-systolic strain. The total systolic strain was defined as the extent of strain between peak systole and peak atrial systole (late ventricular diastole). This represents the total extent of systolic shortening, and is a negative value because it reflects myocardial contraction.

The early-diastolic strain rate was defined as the slope over the duration from end-systole to mid-diastole. The mid-diastolic strain rate was defined as the slope from mid-diastole to the beginning of atrial systole. The percent lengthening subsequent to atrial systole was defined as the ratio of atrial strain (strain from the onset of atrial systole to peak atrial systole) to the total systolic strain. The middiastolic strain rate and the percent lengthening subsequent to atrial systole were indicators of mid- and late-diastolic filling.

Statistical Analysis

All values are reported as mean ± standard deviation (SD). A Student's *t*-test was used to compare NVs and patients with FHC. A value of $P < 0.05$ was considered significant.

RESULTS

Images

The images show tag persistence during the entire cardiac cycle, and also exhibit the black-blood nature of CSPAMM. If a typical prospectively gated sequence with a 10–20% trigger window had been used, acquisition of the last three to six frames of the full 30 frames acquired would not have been possible. In cine loops of all acquired frames, cardiac motion subsequent to atrial systole is evident in the late cardiac phases.

Regional LV Function

A sample E_{CC} curve representing function in an NV and a patient with FHC is shown in Fig. 1. The NV curve in Fig. 1 exhibits all phases of the cardiac cycle, including rapid shortening (systole), rapid lengthening (early diastole), slow lengthening (diastasis), and the ventricular response to atrial systole. The FHC patient curve in Fig. 1 exhibits dynamics that are distinctly different from the NV curve. Early shortening is similar, but total systolic shortening is reduced; early-diastolic lengthening is slower, and no period of diastasis is observed; and the ventricular response to atrial systole is still evident as a strain exceeding the end-diastolic reference. At the level of the tagged image acquisition, through-plane motion was measured to average 2.8 ± 1.8 mm. The strain curves for each short-axis tagged slice show no significant apex-to-base gradient, indicating that the function across the imaged slices was not significantly different.

Values for all measured indices of ventricular function are tabulated in Tables 2 and 3. The total systolic strains (Table 2) attained by the FHC subject group were lower than the NV group in septal and inferior wall segments ($P < 0.01$). Total systolic strain in the anterior and lateral regions of the FHC population was decreased, but not statistically different than that in the NV population. Early-diastolic strains (Table 2) were reduced compared to the NV group in all segments ($P < 0.01$). Mid-diastolic strains (Table 2) were increased in all segments, but because of the wide variability between patients, these changes did not reach statistical significance. The strain subsequent to atrial systole (Table 2) increased in all segments, especially laterally ($P < 0.01$). Figure 1 demonstrates that the acquisition delay due to QRS detection and tagging pulses results in significant systolic shortening prior to acquisition of the first image. Without full-cycle imaging, total systolic strains would be underestimated by 17% in NVs and 32% in FHC patients ($P < 0.01$ for all regions).

Although systolic strain rates (Table 3) expressed as midwall circumferential strain per second were decreased in the FHC group, they were not significantly different between the two groups in any region. Early-diastolic strain rates (Table 3) expressed as midwall circumferential strain per second, were significantly decreased for all regions in the patients with FHC ($P < 0.01$). Trends toward higher mid-diastolic strain rates (Table 3) were found in all regions for patients with FHC, indicating a lack of true diastasis. All measures of ventricular diastolic function deviated from normal in the direction expected for patients with impaired diastolic function.

The percent lengthening subsequent to atrial systole (Table 3) was significantly increased in the septal ($P < 0.03$), lateral ($P < 0.01$), and inferior walls ($P < 0.05$) of FHC patients, and a similar trend was found in the anterior wall. Both the mid-diastolic strain rates and the percent lengthening subsequent to atrial systole were shown to increase in patients with FHC, indicating a greater dependence on atrial systole for total diastolic lengthening.

Septal and inferior early-diastolic strain rates were significantly lower than anterior early-diastolic strain rates within the FHC patients ($P < 0.01$ and $P < 0.03$, respectively). In addition, septal and inferior early-diastolic strain rates were lower than lateral early-diastolic strain rates ($P < 0.08$ (NS) and $P < 0.05$, respectively). In the NVs, significant decreases in early-diastolic

strain rates were seen between the septal and anterior segments and lateral and inferior segments (all $P < 0.02$).

Wall thicknesses in FHC patients were significantly thicker than those in the NVs on a regional basis (all $P < 0.001$). As listed in Table 1, the maximal LV end-diastolic wall thickness in patients with FHC averaged 25 ± 2 mm. Significant regional correlations were found between end-diastolic wall thickness and both early-diastolic strain and early-diastolic strain rate for both FHC patients and NVs in all four segments individually and when summarized as a global average. For example, in the septum, the correlation between end-diastolic wall thickness and early-diastolic strain was $y = -0.01x + 0.20$, $r = -0.8$. In the septum, the correlation between end-diastolic wall thickness and early-diastolic strain rate was $y = -0.03x + 0.92$, $r = -0.75$.

DISCUSSION

A quantitative analysis of regional contractile function in patients with FHC demonstrated significant differences in systolic and diastolic function compared with normal subjects. The MRI technique introduced here provided noninvasive, quantitative, regional function measurements across the entire cardiac cycle. In particular, abnormalities in early-diastolic relaxation, mid-diastole, and late-diastole were all significantly different between NVs and patients with FHC. Without full-cycle imaging, total systolic strains are significantly underestimated.

The reductions in the early-diastolic strain rates and increases in mid-diastolic strain rates seen in patients with FHC were consistent with previously obtained global measures of diastolic filling and pressure decay (18,19). Reduction of early-diastolic strain rates reflected a prolonged and slower filling phase during early diastole. This slow filling phase continued into late diastole, as reflected by the increase in the mid-diastolic strain rate. Reductions in early-diastolic strains, and increases in mid-diastolic strains indicate slow and impaired filling in the patients with FHC relative to the NVs.

The CAPTOR/CSPAMM technique with an echo-train readout allows the acquisition of 30 phases during the entire cardiac cycle, which was shown to be adequate for characterizing rapid events, such as early diastole. This temporal resolution resulted in four to six images over the early (rapid) filling phase, which was sufficient to demonstrate statistically different strain rates in the two studied populations. Systolic strain rates measured in patients with FHC were reduced, but were not statistically different from measures obtained in NVs, indicating similar early-systolic function. Assessment of total systolic strains revealed significant differences between NVs and patients with FHC in septal and inferior walls, but not in the anterior or lateral walls. Increased strains (relative to the septum) in the lateral wall have been observed by others in both NVs (3,4) and patients with FHC (6,7), suggesting there is a regional heterogeneity of function in NVs and patients with FHC. Early-diastolic strain rates showed significant regional heterogeneity. Furthermore, greater hypertrophy correlated with poorer diastolic function.

Some limitations should be considered. Acquiring each direction of stripe tags in separate breath-holds may introduce errors in quantification of regional strain; however, this is more feasible than using the longer breath-holds needed to obtain both in a single acquisition. Although through-plane motion was shown to be limited in FHC patients, collecting more short- and long-axis slices would allow further characterization of this disease. The small sample size of the current study limited our ability to make regional comparisons with other diastolic parameters, such as the transmitral filling velocities.

CONCLUSIONS

In conclusion, the CSPAMM/CAPTOR technique enables regional indices of myocardial function to be quantified during all phases of the cardiac cycle. This technique reveals regional systolic and diastolic impairment in patients with FHC.

ACKNOWLEDGMENTS

The authors thank Dr. Kwabena Agyeman for help with the patient scans.

Grant sponsor: National Heart, Lung, and Blood Institute, National Institutes of Health.

REFERENCES

1. Reichek N. MRI myocardial tagging. J Magn Reson Imaging 1999;10:609–616. [PubMed: 10548769]
2. Moore CC, McVeigh ER, Zerhouni EA. Quantitative tagged magnetic resonance imaging of the normal human left ventricle. Top Magn Reson Imaging 2000;11:359–371. [PubMed: 11153703]
3. Moore CC, Lugo-Olivieri CH, McVeigh ER, Zerhouni EA. Three-dimensional systolic strain patterns in the normal human left ventricle: characterization with tagged MR imaging. Radiology 2000;214:453–466. [PubMed: 10671594]
4. Bogaert J, Rademakers FE. Regional nonuniformity of normal adult human left ventricle. Am J Physiol Heart Circ Physiol 2001;280:H610–H620. [PubMed: 11158958]
5. Maier SE, Fischer SE, McKinnon GC, Hess OM, Krayenbuehl HP, Boesiger P. Evaluation of left ventricular segmental wall motion in hypertrophic cardiomyopathy with myocardial tagging. Circulation 1992;86:1919–1928. [PubMed: 1451263]
6. Kramer CM, Reichek N, Ferrari VA, Theobald T, Dawson J, Axel L. Regional heterogeneity of function in hypertrophic cardiomyopathy. Circulation 1994;90:186–194. [PubMed: 8025995]
7. Young AA, Kramer CM, Ferrari VA, Axel L, Reichek N. Three-dimensional left ventricular deformation in hypertrophic cardiomyopathy. Circulation 1994;90:854–867. [PubMed: 8044957]
8. Stuber M, Scheidegger MB, Fischer SE, Nagel E, Steinemann F, Hess OM, Boesiger P. Alterations in the local myocardial motion pattern in patients suffering from pressure overload due to aortic stenosis. Circulation 1999;100:361–368. [PubMed: 10421595]
9. Nagel E, Stuber M, Lakatos M, Scheidegger MB, Boesiger P, Hess OM. Cardiac rotation and relaxation after anterolateral myocardial infarction. Coron Artery Dis 2000;11:261–267. [PubMed: 10832560]
10. Fischer SE, McKinnon GC, Maier SE, Boesiger P. Improved myocardial tagging contrast. Magn Reson Med 1993;30:191–200. [PubMed: 8366800]
11. Feinstein JA, Epstein FH, Arai AE, Foo TK, Hartley MR, Balaban RS, Wolff SD. Using cardiac phase to order reconstruction (CAPTOR): a method to improve diastolic images. J Magn Reson Imaging 1997;7:794–798. [PubMed: 9307903]
12. Epstein FH, Wolff SD, Arai AE. Segmented k-space fast cardiac imaging using an echo-train readout. Magn Reson Med 1999;41:609–613. [PubMed: 10204886]
13. Reeder SB, Atalar E, Faranesh AZ, McVeigh ER. Multi-echo segmented k-space imaging: an optimized hybrid sequence for ultrafast cardiac imaging. Magn Reson Med 1999;41:375–385. [PubMed: 10080287]
14. MacFall JR, Pelc NJ, Vavrek RM. Correction of spatially dependent phase shifts for partial Fourier imaging. Magn Reson Imaging 1988;6:143–155. [PubMed: 3374286]
15. Shechter G, Ozturk C, McVeigh ER. Interactive four-dimensional segmentation of multiple image sets. Proc SPIE 2000;3976:165–173.
16. Guttman MA, Zerhouni EA, McVeigh ER. Analysis and visualization of cardiac function from MR images. IEEE Comput Graph Appl 1997;17:30–38.
17. Ozturk C, McVeigh ER. Four-dimensional B-spline based motion analysis of tagged MR images: introduction and in vivo validation. Phys Med Biol 2000;45:1683–1702. [PubMed: 10870718]
18. Betocchi S, Bonow RO, Bacharach SL, Rosing DR, Maron BJ, Green MV. Isovolumic relaxation period in hypertrophic cardiomyopathy: assessment by radionuclide angiography. J Am Coll Cardiol 1986;7:74–81. [PubMed: 3941220]

19. Briguori C, Betocchi S, Losi MA, Manganelli F, Piscione F, Pace L, Boccalatte M, Gottilla R, Salvatore M, Chiariello M. Noninvasive evaluation of left ventricular diastolic function in hypertrophic cardiomyopathy. Am J Cardiol 1998;81:180–187. [PubMed: 9591902]

20. Lorenz CH, Walker ES, Morgan VL, Klein SS, Graham TP Jr. Normal human right and left ventricular mass, systolic function, and gender differences by cine magnetic resonance imaging. J Cardiovasc Magn Reson 1999;1:7–21. [PubMed: 11550343]

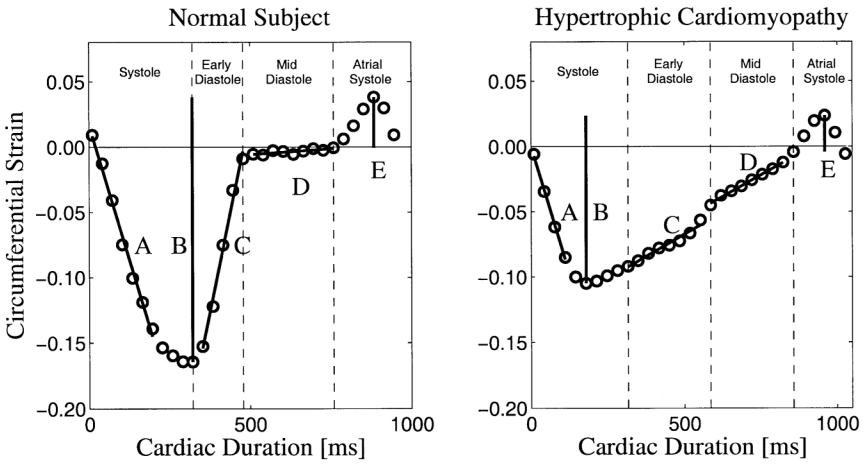

FIG. 1.

A sample curve of the LV midwall circumferential strain in the inferior wall. Indices of cardiac function are shown: A, systolic strain rate; B, total systolic strain; C, early-diastolic strain rate; D, mid-diastolic strain rate; and E, lengthening subsequent to atrial systole. Measures B and E were used to calculate the percent lengthening subsequent to atrial systole, defined as E/B.

Table 1

Left Ventricular Measures From Cine MRI

Patient	LV mass (g)	Wall thickness (mm)				
		Sep	Ant	Lat	Inf	Maximum
1	469	22	20	22	23	27
2	393	19	21	14	16	25
3	297	17	17	19	21	25
4	258	13	15	10	14	26
5	233	20	12	13	21	27
6	276	19	17	15	16	23
7	389	22	20	25	22	26
8	184	15	12	11	11	20
Mean ± SD	312 ± 96	18 ± 3	17 ± 4	16 ± 5	18 ± 4	25 ± 2

The maximal LV wall thickness was measured on the short axis slice with the most severe hypertrophy. Other measurements were all at the mid-ventricular level. Normal LV wall thickness is 6–12 mm and normal LV mass is < 234 g (20). Sep, septal wall; Ant, anterior wall; Lat, lateral wall; Inf, inferior wall.

Table 2

Decomposition of LV Circumferential Strains

		Controls (N = 6)	FHC (N = 8)	*P* value
Total systolic strain	Septal	−19.5 ± 2.3	−13.4 ± 4.7	<0.01
	Anterior	−20.1 ± 1.8	−17.7 ± 3.0	NS
	Lateral	−22.0 ± 3.5	−17.4 ± 4.3	NS
	Inferior	−22.5 ± 3.2	−15.2 ± 3.6	<0.01
Early diastolic strain	Septal	13.8 ± 1.8	4.7 ± 3.4	<0.01
	Anterior	14.5 ± 1.4	7.8 ± 4.3	<0.01
	Lateral	16.0 ± 2.8	7.4 ± 4.7	<0.01
	Inferior	16.7 ± 3.0	6.3 ± 5.2	<0.01
Mid-diastolic strain	Septal	2.9 ± 0.7	3.2 ± 1.4	NS
	Anterior	2.0 ± 0.8	3.6 ± 1.6	NS
	Lateral	2.2 ± 0.8	2.7 ± 1.5	NS
	Inferior	1.5 ± 0.8	3.2 ± 2.0	NS
Atrial systolic strain	Septal	2.8 ± 1.1	4.4 ± 3.1	NS
	Anterior	3.5 ± 0.8	5.1 ± 3.0	NS
	Lateral	3.8 ± 0.4	6.1 ± 2.1	<0.01
	Inferior	4.2 ± 1.0	4.7 ± 2.5	NS

Table 3

Systolic and Diastolic Strain Rates and Percent Lengthening Subsequent to Atrial Systole (PLSAS)

		Controls (N = 6)	FHC (N = 8)	*P* value
Systolic strain rate (E_{cc}/s)	Septal	−71.8 ± 9.4	−61.3 ± 18.8	NS
	Anterior	−74.8 ± 4.9	−72.3 ± 10.6	NS
	Lateral	−71.2 ± 13.8	−66.3 ± 13.1	NS
	Inferior	−74.0 ± 9.6	−60.7 ± 16.0	NS
Early diastolic strain rate (E_{cc}/s)	Septal	72.2 ± 11.9	29.2 ± 24.1	<0.01
	Anterior	73.9 ± 3.2	54.6 ± 20.0	<0.03
	Lateral	108.2 ± 12.9	53.5 ± 26.4	<0.01
	Inferior	110.8 ± 10.7	35.3 ± 26.0	<0.01
Mid-diastolic strain rate (E_{cc}/s)	Septal	9.3 ± 10.0	21.0 ± 22.2	NS
	Anterior	6.2 ± 2.5	25.0 ± 18.3	NS
	Lateral	7.3 ± 12.2	19.2 ± 28.4	NS
	Inferior	4.2 ± 18.6	22.3 ± 23.4	NS
Percent lengthening subsequent to atrial systole	Septal	14.0 ± 4.8	30.7 ± 17.1	<0.03
	Anterior	17.8 ± 4.3	29.2 ± 16.5	NS
	Lateral	17.4 ± 1.8	36.7 ± 12.5	<0.01
	Inferior	18.7 ± 3.2	32.4 ± 16.6	<0.05

NS, not significant.